AGU PUBLICATIONS

JGR

Journal of Geophysical Research: Oceans

RESEARCH ARTICLE

10.1002/2014JC010312

Key Points:
- Nodal variations were estimated and compared with equilibrium tidal theory
- Nodal cycle was found in S2
- Significant trends were found in semidiurnal tides

Supporting Information:
- Readme
- Auxiliary Material Revised

Correspondence to:
X. Feng,
xiangbo.feng@soton.ac.uk

Citation:
Feng, X., M. N. Tsimplis, and P. L. Woodworth (2015), Nodal variations and long-term changes in the main tides on the coasts of China, *J. Geophys. Res. Oceans*, *120*, 1215–1232, doi:10.1002/2014JC010312.

Received 11 JUL 2014
Accepted 28 JAN 2015
Accepted article online 3 FEB 2015
Published online 23 FEB 2015
Corrected on 13 MAR 2015

This article was corrected on 13 MAR 2015. See the end of the full text for details.

Nodal variations and long-term changes in the main tides on the coasts of China

Xiangbo Feng[1,2], Michael N. Tsimplis[1], and Philip L. Woodworth[3]

[1]National Oceanography Centre, Southampton, UK, [2]State Key Laboratory of Hydrology-Water Resources and Hydraulic Engineering, Hohai University, Nanjing, China, [3]National Oceanography Centre, Liverpool, UK

Abstract The long-term changes in the main tidal constituents (O_1, K_1, M_2, N_2, and S_2) along the coasts of China and in adjacent seas are investigated based on 17 tide-gauge records covering the period 1954–2012. The observed 18.61 year nodal modulations of the diurnal constituents O_1 and K_1 are in agreement with the equilibrium tidal theory, except in the South China Sea. The observed modulations of the M_2 and N_2 amplitudes are smaller than theoretically predicted at the northern stations and larger at the southern stations. The discrepancies between the theoretically predicted nodal variations and the observations are discussed. The 8.85 year perigean cycle is identifiable in the N_2 parameters at most stations, except those in the South China Sea. The radiational component of S_2 contributes on average 16% of the observed S_2 except in the Gulf of Tonkin, on the south coast, where it accounts for up to 65%. We confirmed the existence of nodal modulation in S_2, which is stronger on the north coast. The semidiurnal tidal parameters show significant secular trends in the Bohai and Yellow Seas, on the north coast, and in the Taiwan Strait. The largest increase is found for M_2 for which the amplitude increases by 4–7 mm/yr in the Yellow Sea. The potential causes for the linear trends in tidal constants are discussed.

1. Introduction

The nodal cycle is the main long-term modulation of lunar tidal parameters. It is caused by the precession of the lunar ascending node that has a period of 18.61 years. The late 19th century saw the development of the harmonic analysis of tidal observations [*Darwin and Adams*, 1883], in which the nodal cycle was initially referred to as "*reduction*," representing the apparent variations in amplitude and phase of the main tidal components because of the impossibility of including in annual analyses all the satellites that are in the tidal potential. *Doodson* [1928] refined the method of calculating "*nodal factors*" which determine the nodal variations of amplitude and phase of each tidal component. *Pugh and Woodworth* [2014] include a description of nodal variations in the equilibrium tide, while *Haigh et al*. [2011] have mapped the worldwide distribution of nodal variations for the major tidal components using a numerical tidal model.

Deviations from the equilibrium theory have been identified in several regions around the world. The observed nodal modulation of M_2 amplitude has been found to be less than that predicted by the equilibrium theory along the British Isles coasts [*Amin*, 1983, 1985; *Woodworth et al*., 1991; *Woodworth*, 2010], the western coast of Australia [*Amin*, 1993; *Woodworth*, 2010], and the Bay of Fundy and Gulf of Maine [*Ku et al*., 1985; *Ray*, 2006; *Müller*, 2011]. The differences have been suggested to be caused by the effect of bottom friction on the tidal signal [*Ku et al*., 1985; *Pingree and Griffiths*, 1987]. By contrast, along the coasts of the Mediterranean and the Caribbean Seas, the nodal modulations of the main lunar constituents were found to follow the equilibrium tidal theory [*Shaw and Tsimplis*, 2010; *Torres and Tsimplis*, 2011]. The differences in these results correspond to the size of the tidal signal, with the latter studies referring to regions with small tides. A study based on altimetry data suggests that in the Pacific and western Atlantic Oceans the observed nodal amplitudes for main tidal constituents are in general close to the theoretical equilibrium values, but tend to exceed theory where the nodal amplitudes are small [*Cherniawsky et al*., 2010].

The S_2 tide is primarily generated by the solar gravitational potential. Thus, its amplitude and phase are, in principle, not expected to be affected by the lunar nodal cycle. However, variations of 1–2% in S_2 amplitude at the nodal frequency were found from interannual analyses on UK coasts and the Gulf of Maine, as well as

on western Australian coasts [*Amin*, 1983, 1993; *Woodworth*, 2010; *Müller*, 2011]. The nonlinear interaction with M_2 has been suggested to be the cause of such long-term variation [*Woodworth*, 2010]. In addition to the gravitational forcing of S_2, oscillations in barometric pressure, changes in ocean temperature, and onshore-offshore wind have also been argued as contributing to the sea surface variations at the S_2 frequency [*Chapman and Lindzen*, 1970; *Zetler*, 1971; *Pugh and Woodworth*, 2014]. The nongravitational component of S_2 is called the radiational tide and its amplitude has been estimated to be 10–18% of the gravitational amplitude, depending on geographical region and the physical parameters concerned (e.g., pressure, wind stress, and/or thermal forcing) [*Cartwright*, 1968; *Zetler*, 1971; *Amin*, 1982; *Arbic*, 2005].

Linear trends in the amplitude and phase of tidal constituents have been identified around the British Isles [*Amin*, 1983], southern North Sea [*Hollebrandse*, 2005], Gulf of Maine [*Ray*, 2006], Northwest America [*Jay*, 2009], North Atlantic [*Müller*, 2011], Caribbean Sea [*Torres and Tsimplis*, 2011], and East China Sea [*Feng and Tsimplis*, 2014]. The largest rate reported is $\sim$7 mm/yr for the M_2 amplitude occurring at Lianyungang on the west coast of the Yellow Sea [*Feng and Tsimplis*, 2014]. *Woodworth* [2010] and *Müller et al*. [2011] analyzed the spatial distribution of the observed trends in the major tidal constituents and found that the linear changes are commonplace for the North American coasts. S_2 was found to be the component that usually shows the largest linear changes among the main tidal constituents [*Müller et al*., 2011].

Why tidal components change linearly with time is not well understood. Changes in mean sea level have been argued as being able to distort the propagation of tidal waves [*Amin*, 1983], and the resulting changes in the tide have been estimated on the basis of numerical models [*Amin*, 1983; *Green*, 2010; *Pickering et al*., 2012]. In general, the model estimates are small and unable to explain fully the observed tidal changes on the American and European coasts [*Jay*, 2009; *Müller et al*., 2011]. Changes in the coastal morphology and bathymetry due to natural processes and anthropogenic works have also been argued as being the cause of changes in the tide in the Bohai Sea [*Pelling et al*., 2013]. *Ray* [2009] argued that the decrease in the S_2 amplitude on the east coast of North America could be due to changes in the radiational forcing. *Woodworth* [2010], *Müller et al*. [2011], and *Müller* [2011, 2012] discussed additional potential causes, for example, changes in the tidal potential, atmospheric dynamics, ocean circulation, stratification conditions, and thermocline depths. However, the causes for most of observed changes remain unclear.

In the marginal seas adjacent to China, spatial features of the main tidal signals have been identified from numerical models [*Kang et al*., 1998; *Fang et al*., 1999; *Lefèvre et al*., 2000; *Fang et al*., 2004], tide gauges [*Fang*, 1986, 1994], and satellite observations [*Hu et al*., 2001], in which the nodal variations are assumed to follow the equilibrium tidal theory. However, in this shallow-water region (usually less than 100 m, see Figure 1a) the bottom friction effect on tides has been well recognized [*Kang et al*., 1998; *Lefèvre et al*., 2000; *He et al*., 2004], and this effect in other regions has been found to be capable of altering the nodal behavior of tides from that expected, such as those mentioned above. Thus, it is worthwhile to investigate the observed nodal variations of tides in the China seas, and to compare them with the equilibrium tidal theory.

The Chinese coasts are being heavily modified due to sediment deposition at river mouths [*Chu et al*., 2006; *Pelling et al*., 2013], coastal erosion because of the impact of frequent tropical cyclones [*Qi et al*., 2010; *Feng et al*., 2012; *Feng and Tsimplis*, 2014], and extensive tidal flat reclamation that has taken place over the past few decades [*Li et al*., 2004; *Wang et al*., 2011; *Li et al*., 2013; *Wang et al*., 2014]. To our knowledge, there are no published papers describing the long-term trends in tides in this region, despite their importance for coastal planning.

In this paper, the 18.61 year nodal modulations of the main tidal constituents for the Chinese coasts are estimated from observations and compared with the equilibrium theory. Trends in tidal constituents are also mapped. The paper is organized in five sections. The data processing of sea level records and the methodology used for empirically fitting the nodal modulations are described in section 2. In section 3, the observed nodal modulations and linear trends of the main tidal constituents (O_1, K_1, M_2, N_2, and S_2) are presented and the ability of the equilibrium tidal theory to explain the observed changes is discussed. Section 4 discusses the possible causes for the differences between the observed nodal modulations and the equilibrium theory. Furthermore, it discusses the observed linear trends in the tidal components. Finally, our conclusions are presented in section 5.

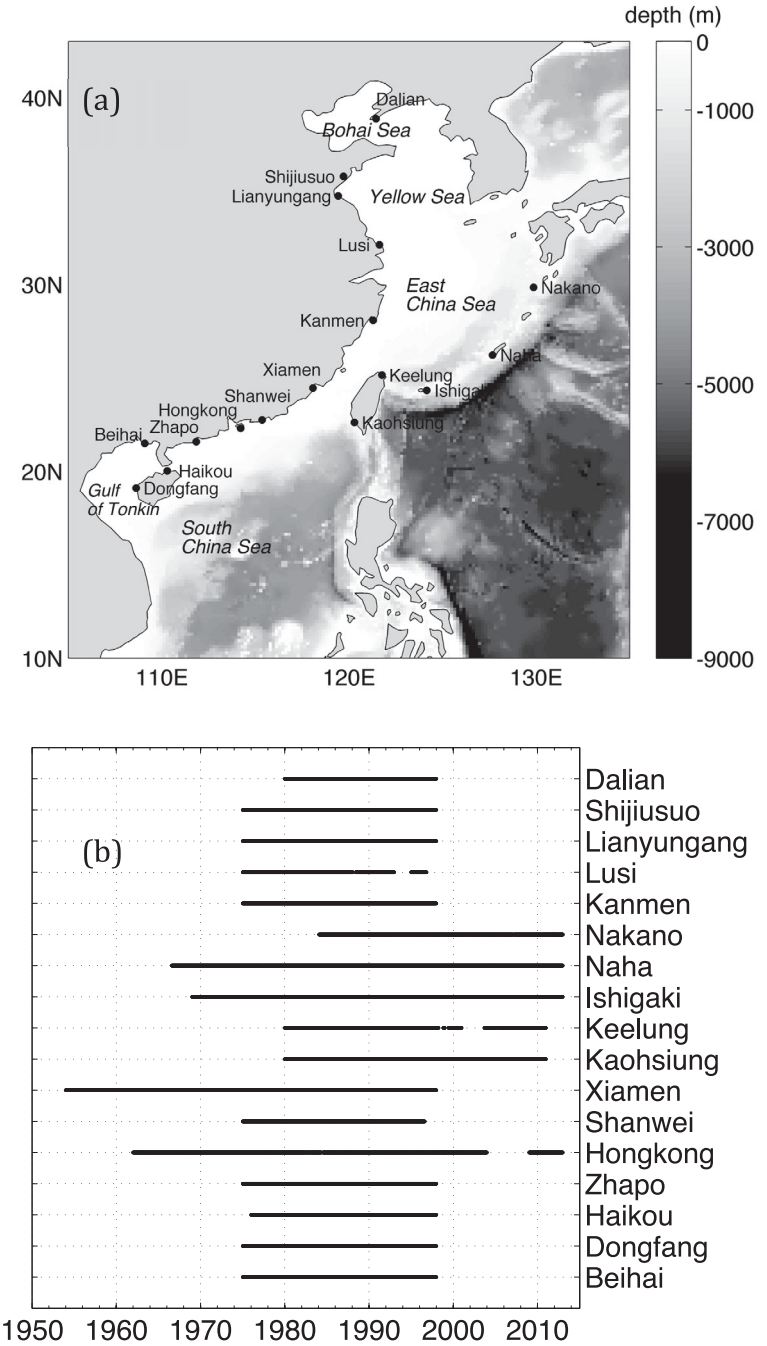

Figure 1. (a) Locations of tide-gauge stations along the seas adjacent to China and (b) corresponding periods of valid data. The bathymetry in the studied areas is also shown in Figure 1a, which is based on the GEBCO_08 Grid data set from the British Oceanographic Data Centre.

2. Data and Methodology

2.1. Sea Level Data

Hourly sea level data from 16 tide gauges on the Chinese coasts and 3 Japanese stations in the East China Sea are used (Figure 1a). The data were obtained from the University of Hawaii Sea Level Center (UHSLC). The sea level data span the period 1954–2012. From the 19 records available, 16 are longer than 23 years (Figure 1b). Two pairs of records were combined leaving 17 records covering at least 18 years for the analysis.

The nearby Dalian and Laohutan stations have data for the periods 1975–1990 and 1991–1997, respectively. However, at Dalian the tide gauge was relocated twice, once at the end of 1976, and once in 1979. After 1979, it shared the same position as Laohutan. Thus, the data for the periods 1980–1990 at Dalian and 1991–1997 at Laohutan were combined.

At Hongkong, the tide gauge was located at North Point for the period 1962–1986, and then moved half a kilometer away to Quarry Bay for the period 1987–2012. The same datum applies to both locations with an offset of 1.02 cm [*Ding et al*., 2001]. Thus, the two Hongkong records were merged into a 51 year record, the longest in the study.

The tidal constituents were estimated annually by using the sea level processing package SLPR2 version 3.0 provided by UHSLC, after the mean value of sea level over the whole period of observations was removed from the record. The tidal analysis program is described in detail in *Foreman* [1977]. A maximum of 68 constituents is allowed in the analysis of 1 year of hourly records. It was required that the difference in tidal frequency between two resolvable tidal constituents is at least one cycle per year. Thus, the Rayleigh criterion was given a value of 1. The tidal amplitude and phase lag for each constituent are expressed as cosine and sine functions, which are estimated in observations by a least squares regression method. When the regression is finished, the difference between the sum of the observation squares and the sum of the predicted tidal curve squares is calculated. This difference is divided by the degrees of freedom providing the squares residual, where the "degrees of freedom" is the difference between the number of hourly observations and the number of functions fit in the analysis. The square root of the squares residual is then used to determine the errors for the tidal parameters. Through this method, the errors in the tidal parameters in each year have approximately the same magnitude.

Note that during the process the equilibrium nodal correction in the program was not applied to any lunar constituent. The annual and semiannual components were not included either, as these are not primarily astronomical in character. The tidal constants for each year, with their estimated errors (standard deviations) as their uncertainty, were then used to estimate the nodal variations and the linear trends for the tidal constituents.

The quality control performed included visual checks of the time series of the hourly measurements and the tidal residuals. Checks were also performed on the estimated annual tidal constants at each station. Values with spurious jumps, datum shifts, and time shifts from the values in other years were excluded. Using this quality control, data in the years 1993 and 1994 at Lusi and 1997 at Shanwei were removed. The periods with valid observations are shown in Figure 1b.

2.2. Lunar Constituent Modulation Model

All lunar constituents are modulated by the 18.61 year nodal cycle, and some of them are also affected by the 8.85 year perigean cycle, e.g., L_2 and N_2. The harmonic parameters of the 18.61 year and the 8.85 year cycles as well as the long-term trends were estimated by a least squares estimation model. The expression of the joint estimation is described as:

$$H_m(t)=\beta_1+\beta_2 t+\beta_2\cos(R_t)+\beta_4\sin(R_t) \tag{1}$$

where $H_m(t)$ is the estimated value of amplitude or phase lag for tidal constituent m, β_1 is the constant value, β_2 is the linear trend, and t the time in units of year. β_3 and β_4 are the amplitudes of the cosine and sine functions of either nodal cycle or perigean cycle, and R_t is the argument of the cosine and sine functions and equal to either the negative of the longitude of the Moon's ascending node (N') (i.e., $N' = -N$) or the longitude of the perigean cycle P [*Doodson and Warburg*, 1941]:

$$\begin{aligned} N' &= 100.8432^\circ + 1934.142^\circ * T - 0.0021^\circ * T^2 \\ P &= 334.3853^\circ + 4069.034^\circ * T - 0.0103^\circ * T^2 \end{aligned} \tag{2}$$

where T is the time t in units of Julian century starting from zero hours at the Greenwich meridian on the first of January 1900.

After fitting equation (1), the estimated mean value of amplitude (or phase lag) ($\bar{B}$), and estimated amplitude ($\alpha_{N' or P}$) and phase lag ($\varphi_{N' or P}$) of the nodal cycle or perigean cycle can be derived as:

Table 1. Nodal Factor (f) and Nodal Angle (u) for Long-Term Modulations of Major Lunar Constituents Derived From the Equilibrium Tidal Theory[a]

	f	u
O_1	1.009 + 0.187 cos(N)	10.8° sin(N)
K_1	1.006 + 0.115 cos(N)	−8.9° sin(N)
M_2, N_2	1.000 – 0.037 cos(N)	−2.1° sin(N)

[a]Note that N is the longitude of lunar ascending node. $N = 0$ in March 1969, November 1987, June 2006, etc., and $N = 180°$ in July 1978, March 1997, October 2015, etc.

$$\bar{B}=\beta_1+\beta_2\bar{t}$$
$$\alpha_{N' \text{ or } P}=\sqrt{\beta_3^2+\beta_4^2} \quad (3)$$
$$\varphi_{N' \text{ or } P}=\tan^{-1}\left(\frac{\beta_4}{\beta_3}\right)$$

where $\bar{t}$ is the time at the middle of record.

The ratio of estimated nodal amplitude over the mean value of tidal amplitude ($\alpha_{N'}/\bar{B}$) expressed as a percentage is also calculated and compared with the theoretical ratio (nodal factor f in Table 1) from the equilibrium tidal theory [*Pugh and Woodworth*, 2014]. Similarly, the estimated nodal amplitude for tidal phase lag is also calculated and compared with that from the theoretical estimate (nodal angle u in Table 1).

The perigean modulation is a third-order term in the tidal potential. The perigean factors are weakly dependent on the latitude (θ) of each station. Based on Doodson's classic expansion method [*Godin*, 1972], the perigean amplitude ratio (the ratio between the perigean change and mean amplitude) ($\alpha_P/\bar{B}$) and the phase factor (φ_P) are expressed as:

$$\alpha_P/\bar{B}=0.085 * \sin(\theta)$$
$$\varphi_P \approx \alpha_P/\bar{B} \quad (4)$$

The value of phase factor (φ_P) in radians is approximately equal to the amplitude ratio ($\alpha_P/\bar{B}$) because of the amplitude ratio $\ll 1$. At stations studied here, the perigean modulation predicted from the equilibrium tidal theory is 2.8–5.3% for the N_2 amplitude and 1.6–3.1° for the phase lag. We also checked the perigean factors based on the tables of *Cartwright and Tayler* [1971] and *Cartwright and Edden* [1973], and found that the difference between the different treatments is very small, less than 0.1% for $\alpha_P/\bar{B}$ and 0.1° for φ_P.

In the first step of fitting the joint model of equation (1), the linear trend (β_2) and the parameters (β_3 and β_4) of the nodal cycle (and the perigean cycle for N_2) were estimated. In next step, if the linear trend (β_2) is not significantly different from zero at the 95% confidence level, the model of equation (1) was reprocessed by omitting the linear trend, while the model was reduced to the linear trend fitting only if the nodal cycle (β_3 and β_4) (and the perigean cycle for N_2) is not statistically significant. The uncertainty in the trend assessment due to errors in the tidal parameters each year was also considered. The linear trend is treated as valid only when the change is still significant when the errors of the series of estimated parameters are taken into account.

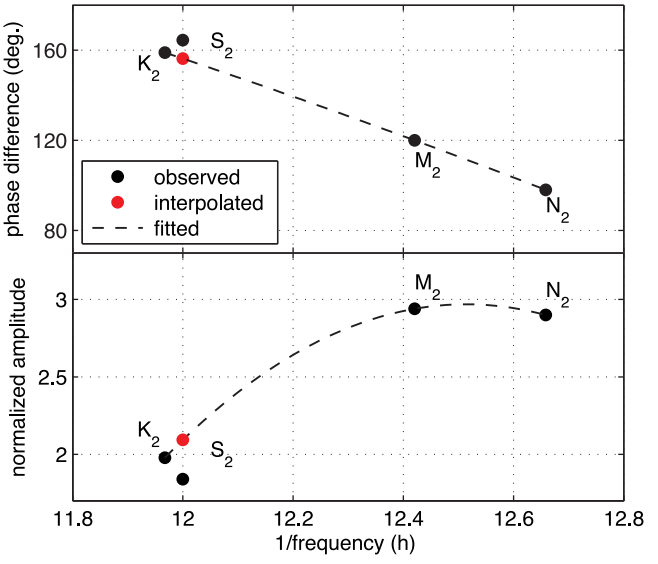

Figure 2. Phase differences and normalized amplitudes relative to the equilibrium tide for K_2, S_2, M_2, and N_2 at Xiamen in 1990. Black dots present the observed values, while the dashed line is the best fit function connecting values of K_2, M_2, and N_2. The red dot is the interpolated value of gravitational S_2 on the fitted line.

2.3. Radiational Component of S_2

For S_2, we separate the response of sea level to radiational forcing from the response to gravitational forcing using the empirical method suggested by *Zetler* [1971]. The method was devised based on the "credo of smoothness" [*Munk and Cartwright*, 1966] which leads to the admittances of tidal constituents within a narrow frequency band being regarded as similar. As a demonstration, Figure 2 shows the phase differences and the ratios

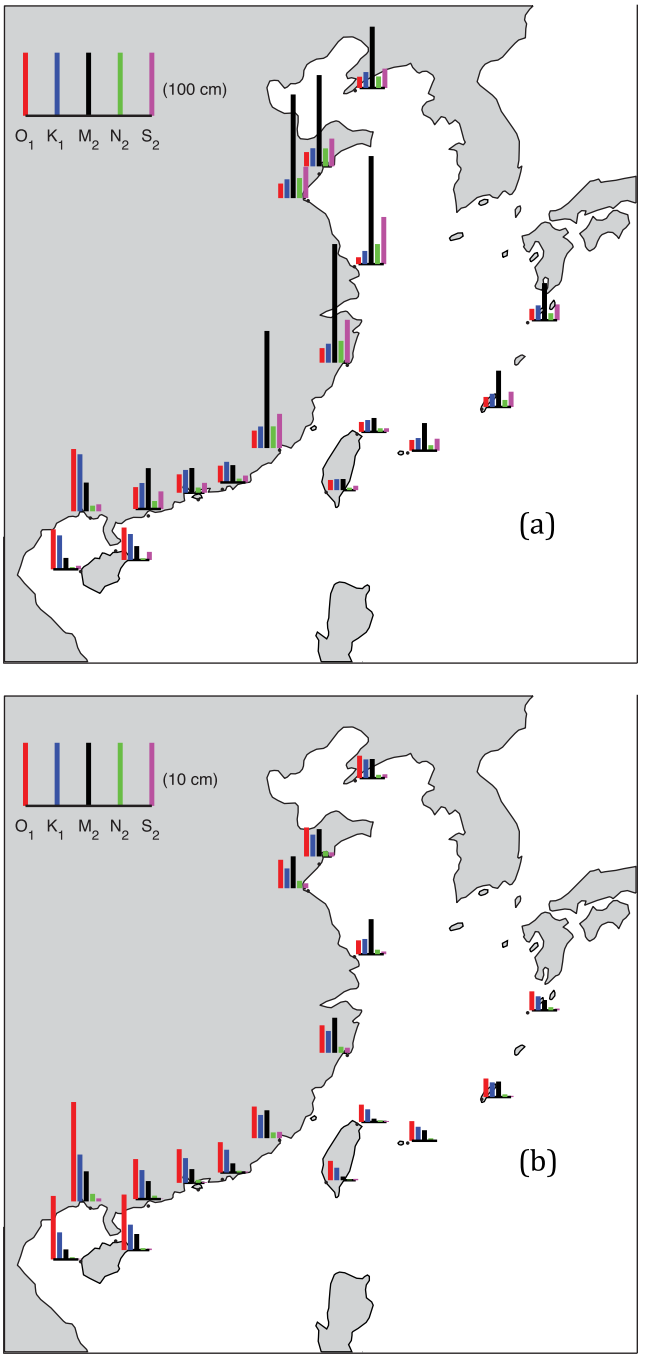

Figure 3. (a) Maps of the mean amplitudes and (b) amplitudes of 18.61 year variations for major tidal constituents O_1, K_1, M_2, N_2, and S_2. The corresponding uncertainty in each value is provided in the supporting information Tables S1–S5.

between the observed and the equilibrium amplitudes (normalized amplitudes) at Xiamen in 1990. The phase difference of N_2, M_2, S_2, and K_2 can be plotted versus a function of frequency by the equilibrium tidal theory. Then, a smooth function of frequency, empirically fitted to the phase differences of N_2, M_2, and K_2, is employed to interpolate to the phase of the gravitational component of S_2 (Figure 2, top). Similarly, another function is used to fit the ratios of the observed amplitude over the equilibrium amplitude for N_2, M_2, and K_2 (Figure 2, bottom). The interpolated ratio at the frequency of S_2 and the equilibrium amplitude of S_2 then gives the amplitude of the gravitational component S_2. Subtracting the gravitational component of S_2 vectorially from the observed S_2 furnishes the radiational component of S_2. This calculation is performed separately for every year of data.

In the above process, the observed parameters of N_2, M_2, and K_2 are treated as the purely gravitational components because the radiational forcing has no influence on the first two constituents and is negligible in the latter [*Chapman and Lindzen*, 1970; *Zetler*, 1971]. Note also that the 18.61 year cycle is removed from the four involved constituents before the calculation is made to avoid the nodal cycle of the lunar constituents influencing the interpolated gravitational S_2.

3. Results

Five major tidal constituents (O_1, K_1, M_2, N_2, and S_2) are analyzed. The mean values ($\bar{B}$), nodal modulation amplitudes ($\alpha_{N'}$), and linear trends (β_2) in the tidal constants as estimated by equation (1) are mapped in Figures 3 and 4. The estimation parameters of equation (1) along with their error bars are provided in the supporting information Tables S1–S5.

3.1. The O_1 and K_1 Components and Their Changes

The mean amplitude ($\bar{B}$) of the main diurnal constituents O_1 and K_1 is in the range 11–98 cm and 16–90 cm, respectively (Figure 3a). The largest values found in the Gulf of Tonkin (Haikou, Dongfang, and Beihai) have

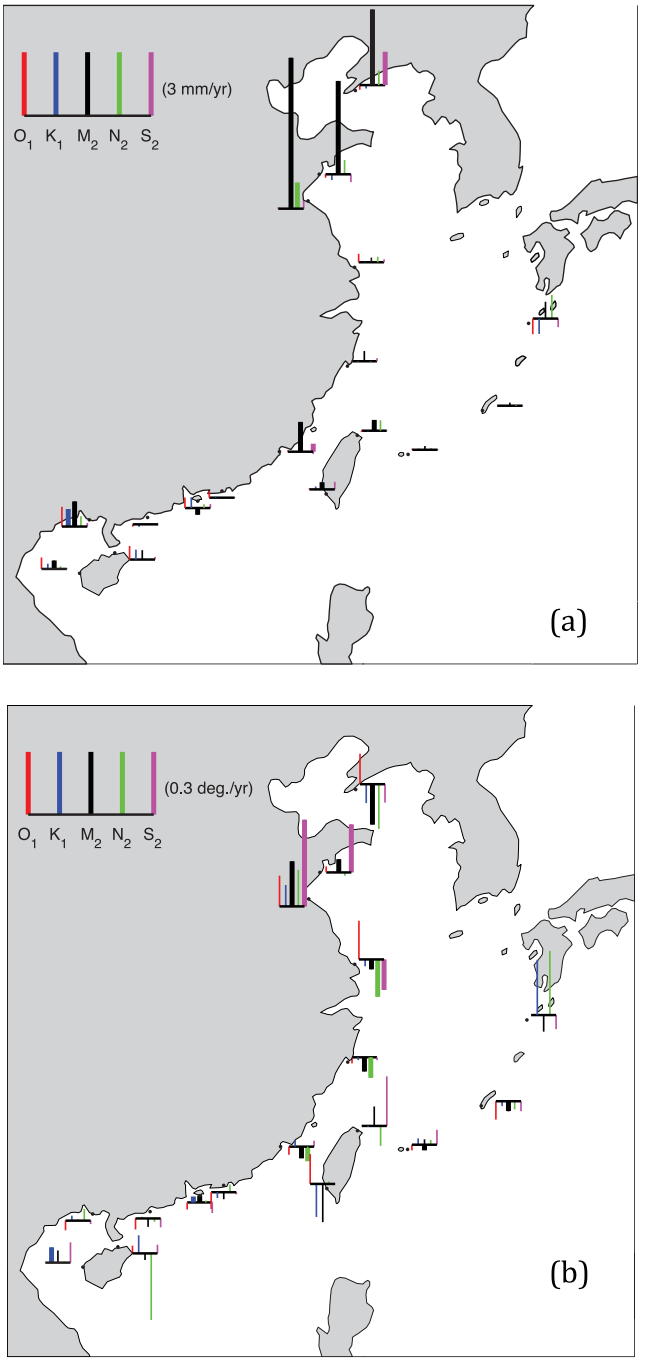

Figure 4. (a) Maps of linear trends of tidal amplitude and (b) phase lag for major tidal constituents O_1, K_1, M_2, N_2, and S_2. The thin bars indicate the trends that do not pass the significance test as described in section 2.2. The corresponding uncertainty in each value is provided in the supporting information Tables S1–S5.

been indicated to be caused by resonance [*Zu et al.*, 2008; *Green*, 2010]. The nodal modulation ($\alpha_{N'}$) is 2.2–15.9 cm for O_1 and 2.0–7.4 cm for K_1 (Figure 3b). In the Gulf of Tonkin, the nodal modulation of O_1 is the strongest signal among the nodal parts of all tidal constituents.

The estimation model accounts for more than 90% of the variance of the O_1 and K_1 amplitudes at all the stations, except at Hongkong for K_1 (82%) (Figures 5a and 5c). There is no phase difference between the theoretical estimate and the estimation model within the range of uncertainty.

The ratio of the observed nodal amplitude over the mean tidal amplitude ($\alpha_{N'}/\bar{B}$) is in agreement with the ratio predicted by the equilibrium theory (18.7% and 11.5% for O_1 and K_1, respectively) at most stations. However, at Hongkong, Dongfang, and Beihai the observed ratio is significantly lower than the theoretically predicted, with values of $16.7 \pm 1.9\%$, $16 \pm 2\%$, and $16 \pm 2\%$ for O_1 and $9 \pm 1\%$, $8.3 \pm 0.6\%$, and $8.2 \pm 0.5\%$ for K_1, respectively. At Beihai, the difference between the predicted and the observed amplitudes is up to 1 cm for O_1 and 3 cm for K_1.

The estimation model accounts for at least 95% of the variance of the phase lag at all stations (Figures 5b and 5d). The predicted amplitude of the nodal cycle of the phase lag (10.8° and 8.9° for O_1 and K_1, respectively) falls into the confidence limits of the observed values ($\alpha_{N'}$) at all stations, except at Shanwei where the observed O_1 modulation is slightly higher than the predicted by 0.4°.

There is no significant trend found in either the amplitude or phase lag of O_1 (Figure 4). The K_1 amplitude has a significant trend of 0.8 ± 0.3 mm/yr at Beihai, and the phase lag shows a significant trend at Hongkong and Dongfang, with a small magnitude of 0.03 ± 0.01°/yr and 0.07 ± 0.05°/yr, respectively.

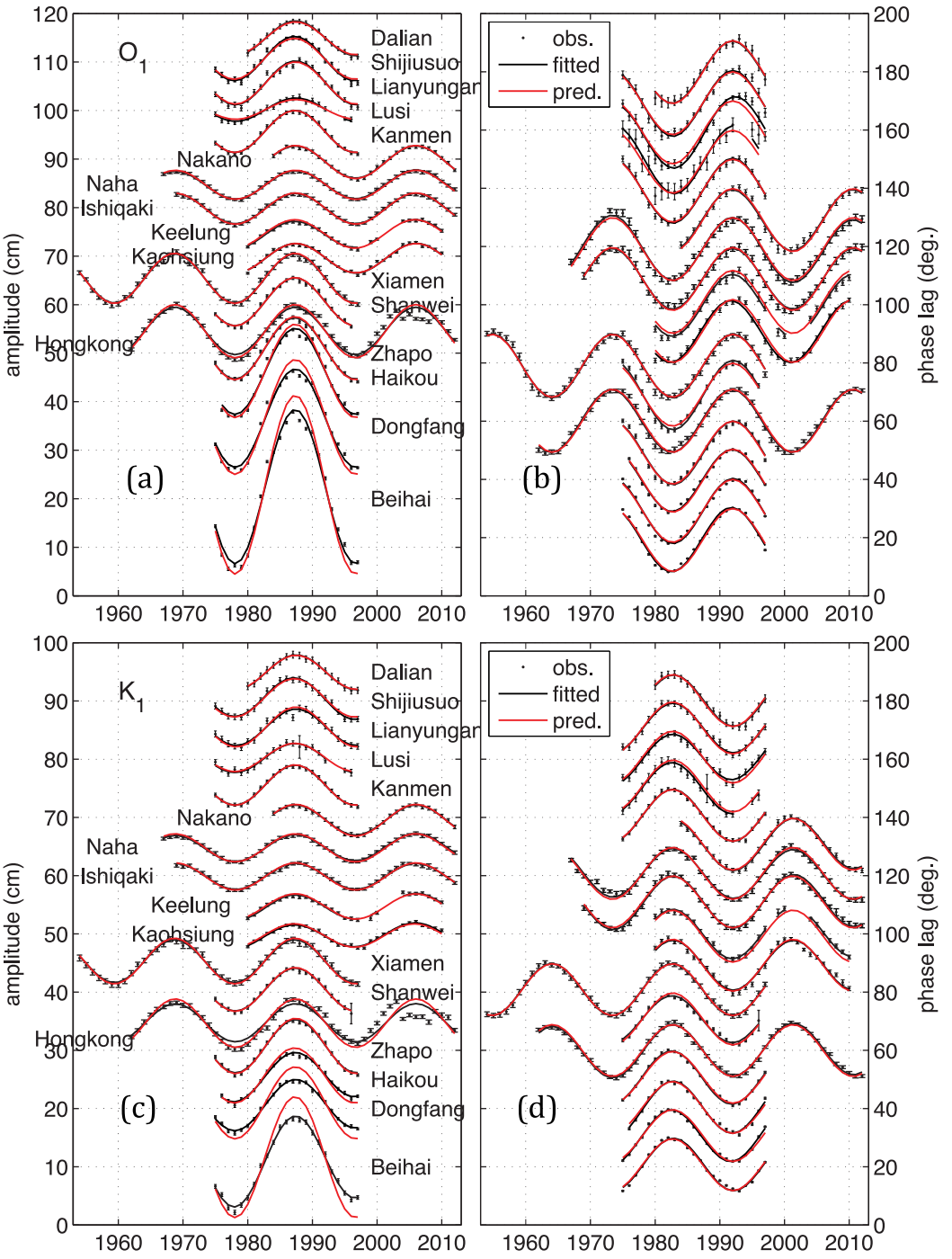

Figure 5. (left) Time series of tidal amplitude and (right) phase lag for major lunar constituents (a and b) O_1 and (c and d) K_1. Black dots present annual values with error bars at 95% confidence level obtained from the harmonic analysis of each 1 year of hourly data. Black and red solid lines are the best fitted curve and theoretical nodal modulation, respectively. Note that the series have been offset for display. Parameters of the best estimations (black solid lines) are presented in the supporting information Tables S1 and S2.

3.2. The M_2 Component and Its Changes

M_2 is the largest tidal constituent along the northern coasts, from Dalian to Xiamen, with the highest amplitude ($\bar{B}$) of 188 cm at Kanmen (Figure 3a) and small values at the southern stations and the islands. The M_2 amplitude at Xianmen (184 cm) is significantly higher than that at the neighboring stations, probably due to wave reflection of the southward propagating tidal wave due to the deep trench in the southern Taiwan

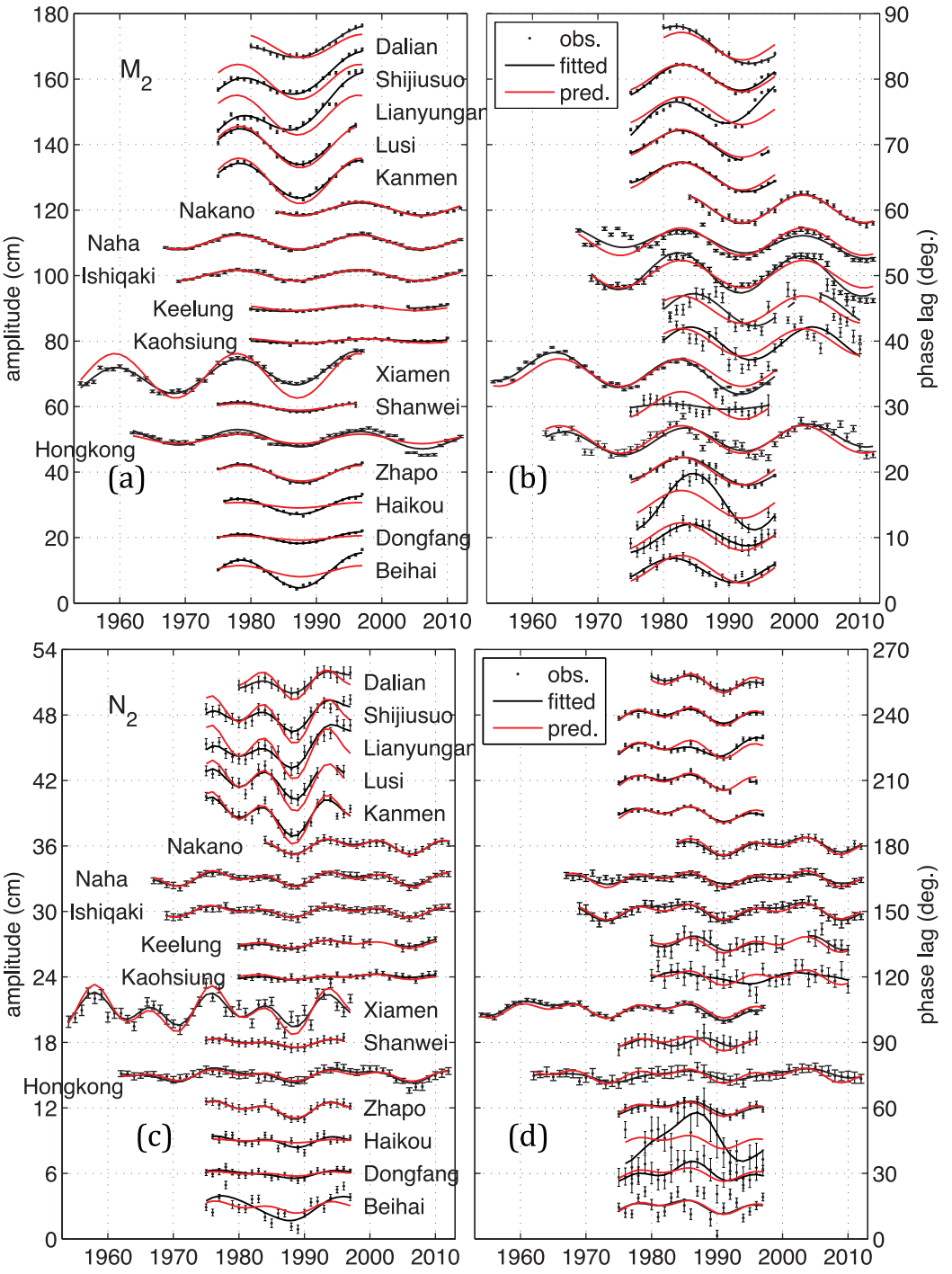

Figure 6. Same as Figure 5, but for (a and b) M_2 and (c and d) N_2. Note that for N_2, the 8.85 year perigean cycle is also involved. Parameters of the best estimations (black solid lines) are listed in the supporting information Tables S3 and S4.

Strait [*Jan et al.*, 2004]. The nodal cycle values ($\alpha_{N'}$) are in range 0.5–5.6 cm, with the highest and lowest values at Kanmen and the Taiwan Island, respectively.

The estimation model accounts for more than 91% of the variance in the M_2 amplitude at all stations, except at Keelung, Kaohsiung, and Hongkong (Figure 6a) where the variance accounted for is 87%, 57%, and 76%, respectively. The low values of M_2 amplitude at the first two stations and the reduction of the M_2 amplitude between 2003 and 2007 at Hongkong (which appear suspect) are associated with the reduced amount of the variance accounted for.

The nodal amplitude ratio of the M_2 amplitude ($\alpha_{N'}/\bar{B}$) is smaller by 0.1–1% (the absolute difference between two percentage values) than that estimated from the equilibrium theory (3.7%) at eight stations in the north of the region (Figure 6a). At the six southernmost stations and Naha, the observed ratios are higher than the expected ratio by 0.4–8.6%. The biggest underestimation by the theory occurs at Haikou, ~3 cm in amplitude. Thus, the equilibrium theory generally overestimates the nodal modulation of the M_2 amplitude in the north but underestimates it in the south.

The percentage of variance accounted for by the estimation model for phase lag is 95% at the stations of the northern mainland coast and 74% at the other stations where low amplitude values are found (Figure 6b). The observed values of the nodal amplitude of the M_2 phase lag ($\alpha_{N'}$) are consistent with the theoretically estimated value of 2.1° at 11 of the 17 stations. However, values 0.1–1.1° lower are found at Kanmen, Naha, and Shanwei, and values 0.1–1.7° higher at Ishiqaki, Xiamen, and Haikou.

The agreement between the estimated and predicted time dependence for the nodal variations of the semidiurnal constituents is worse than that for the diurnal constituents, probably because the nodal signal for modulations of the semidiurnal tides is weaker and the linear trends are larger.

The M_2 amplitude has significant trends at nine stations (Figure 4a). These trends are mostly positive. They are higher at Dalian, Shijiusuo, and Lianyungang with values of 3.6 ± 0.8 mm/yr, 4.4 ± 0.5 mm/yr, and 7.1 ± 0.9 mm/yr, respectively, lower at Xiamen and Beihai with values of 1.4 ± 0.2 mm/yr and 1.2 ± 0.3 mm/yr, respectively, small at Keelung, Kaohsiung, and Dongfang with 0.3–0.5 mm/yr, and negative at Hongkong with -0.3 ± 0.2 mm/yr.

Most tide gauges on the mainland coast have observations for the period 1975–1997. During that period, the trend at Hongkong is 0.5 ± 0.2 mm/yr. No significant difference in the trends between the common period 1975 and 1997 and the extended period are found at Keelung and Kaohsiung. Thus, the negative trends at Hongkong are due to changes before 1975. We conclude that the M_2 amplitude has been increasing along the Chinese coasts between 1975 and 1997, with high rates in the Bohai and Yellow Seas.

There are nine stations with significant trends in the M_2 phase lag, three stations showing positive trends, and six stations showing negative trends (Figure 4b). Five of the nine stations also indicate significant trends in the M_2 amplitude: Dalian, Shijiusuo, Lianyungang, Xiamen, and Hongkong. The higher trends in the M_2 amplitude (over 1.0 mm/yr) coincide with significant changes in the M_2 phase lag.

3.3. The N_2 Component and Its Changes

The mean N_2 amplitude ($\bar{B}$) is 15.5 cm on average, with higher values between 18.4 and 34.8 cm along the northern mainland coast, from Dalian to Xiamen, and smaller values between 2.6 and 12.8 cm in the offshore islands and the South China Sea (Figure 3a). The average nodal and perigean modulation amplitudes ($\alpha_{N'}$ and α_P) are 0.56 and 0.45 cm, respectively, much smaller than the nodal modulations in the other main lunar constituents (Figure 3b). At Dongfang and Beihai, the perigean cycle of N_2 is statistically insignificant.

The estimation model accounts on average for 76% of the N_2 amplitude variance (Figure 6c). The estimation performance is worse in the south where the signal is weaker. The nodal cycle explains on average 17% more variance in the N_2 amplitude than the perigean cycle does at most stations, except at Lusi, Kanmen, and Xiamen where the perigean modulation explains more.

The observed ratio of nodal modulation amplitude ($\alpha_{N'}/\bar{B}$) agrees with the expected value of 3.7% at 11 stations, but is significantly lower at Lusi, Kanmen, and Xiamen by 0.1–0.7% and higher at Hongkong, Dongfang, and Beihai by 1–2.5%. The discrepancy from the theoretical expectation presents a similar spatial pattern as for M_2 with slight underestimations in the north but with significant overestimations in the South China Sea. The observed ratio of the perigean cycle ($\alpha_P/\bar{B}$) is around 3.4% at all stations, except at Naha and Ishiqaki. The observed perigean ratio is lower than the predicted ratio from equation (4) in the north, from Dalian to Ishiqaki by 0.2–1.7%, but consistent with the predicted ratio in the south.

The nodal cycle in the N_2 phase lag is significant at 16 stations except at Beihai, while the perigean cycle is significant at 13 stations except at Kaohsiung, Haikou, Dongfang, and Beihai. The joint estimation model accounts for 67.5% of the variance on average. The nodal cycle explains on average 14.8% more of the variance than the perigean cycle does.

Table 2. Gravitational and Radiational Components of S_2[a]

	Amplitude (cm)				Phase (°)			
Station	Total S_2	Gravitational Component S_2	Radiational Component S_2	Ratio of Radiational Over Gravitational	Total S_2	Gravitational Component S_2	Radiational Component S_2	Difference
Dalian	30.8 ± 0.4	33.6 ± 1.3	4.3 ± 1.1	0.13 ± 0.04	100.2 ± 0.8	94.9 ± 2.3	231.5 ± 16.2	136.7 ± 18.6
Shijiusuo	43.9 ± 0.5	50.1 ± 1.2	8.4 ± 1.1	0.17 ± 0.03	324.6 ± 0.6	318.0 ± 1.6	100.1 ± 8.3	142.1 ± 9.9
Lianyungang	49.7 ± 0.5	56.4 ± 1.4	9.0 ± 1.3	0.16 ± 0.03	343.6 ± 0.5	337.6 ± 1.6	120.9 ± 8.7	143.3 ± 10.4
Lusi	74.8 ± 0.5	81.6 ± 1.4	14.7 ± 1.3	0.18 ± 0.02	156.5 ± 0.4	147.2 ± 1.0	269.0 ± 4.9	121.9 ± 5.9
Kanmen	68.0 ± 0.4	73.1 ± 0.9	8.9 ± 0.9	0.12 ± 0.01	54.7 ± 0.3	48.8 ± 0.8	176.9 ± 5.7	128.1 ± 6.6
Nakano	25.3 ± 0.3	26.8 ± 0.8	3.5 ± 0.7	0.13 ± 0.03	321.3 ± 0.7	314.6 ± 1.7	73.6 ± 12.5	119.0 ± 14.2
Naha	24.1 ± 0.3	25.5 ± 0.7	3.1 ± 0.6	0.12 ± 0.03	327.5 ± 0.6	321.4 ± 1.6	82.8 ± 12.1	121.5 ± 13.7
Ishiqaki	19.0 ± 0.3	19.9 ± 0.8	2.4 ± 0.7	0.12 ± 0.04	329.2 ± 0.9	322.9 ± 2.2	78.0 ± 18.7	115.1 ± 20.9
Keelung	5.5 ± 0.3	5.5 ± 0.7	1.1 ± 0.5	0.19 ± 0.10	40.6 ± 3.2	36.3 ± 8.0	152.6 ± 78.1	116.4 ± 86.1
Kaohsiung	6.9 ± 0.2	7.0 ± 0.6	5.5 ± 2.0	0.78 ± 0.31	351.6 ± 1.5	208.7 ± 97.1	187.6 ± 101.0	339.0 ± 198.0
Xiamen	53.7 ± 0.4	60.8 ± 1.2	9.9 ± 1.1	0.16 ± 0.02	163.8 ± 0.4	157.2 ± 1.3	297.9 ± 6.6	140.7 ± 7.9
Shanwei	11.0 ± 0.3	12.0 ± 0.8	1.4 ± 0.6	0.12 ± 0.06	35.9 ± 1.8	34.6 ± 4.0	200.0 ± 49.0	165.4 ± 53.0
Hongkong	15.6 ± 0.3	17.3 ± 0.8	2.0 ± 0.6	0.12 ± 0.04	26.9 ± 1.2	24.4 ± 2.5	182.6 ± 25.1	158.2 ± 27.7
Zhapo	27.9 ± 0.3	33.3 ± 0.9	9.9 ± 0.8	0.30 ± 0.03	92.8 ± 0.5	77.3 ± 1.7	207.7 ± 4.8	130.5 ± 6.5
Hailkou	13.0 ± 0.2	28.2 ± 0.8	16.0 ± 0.7	0.57 ± 0.07	81.4 ± 1.0	66.9 ± 1.6	235.0 ± 2.4	168.2 ± 4.0
Dongfang	5.6 ± 0.3	10.3 ± 0.7	6.7 ± 0.6	0.65 ± 0.17	237.8 ± 2.7	201.0 ± 3.9	330.5 ± 70.6	129.5 ± 74.5
Beihai	11.1 ± 0.3	29.5 ± 0.8	18.8 ± 0.7	0.64 ± 0.10	341.7 ± 1.4	10.2 ± 1.6	197.7 ± 2.2	187.5 ± 3.8

[a]Note that the nodal cycle of the tidal constituents involved in the estimation has been removed.

Excluding stations where the nodal cycle is not statistically significant, the observed nodal amplitude of the N_2 phase lag is in agreement with the theoretically predicted 2.1° at most stations (12 stations), except at Ishiqaki, Xiamen, and Haikou where the theoretical estimate underestimates the phase lag variations by 0.1–4.3° and at Naha where it overestimates the phase lag variations by 0.1° (Figure 6d and see supporting information Table S4b for more details). The significant perigean modulations of the phase lag are all around 1.7° except at Hongkong, and are lower than the perigean modulation suggested by the equilibrium theory.

The only significant trend in the N_2 amplitude is found at Lianyungang, with an increase of 1.2 ± 0.4 mm/yr (Figure 4a). Linear trends in the N_2 phase lag are found at Lusi, Kanmen, and Xiamen, with rates of −0.2 ± 0.1°/yr, −0.09 ± 0.05°/yr, and −0.07 ± 0.03°/yr, respectively (Figure 4b). Note that where the N_2 constants linearly change the M_2 parameters also change.

3.4. The S_2 Component and Its Changes

S_2 shows a spatial pattern similar to M_2. The mean amplitude ($\bar{B}$) has higher values of 30.8–74.8 cm along the northern mainland coast, and lower values of 5.5–27.8 cm on the south coast and at the offshore islands (Figure 3a). The highest and lowest values of $\bar{B}$ occur at Lusi and Keelung, respectively.

The radiational part of the S_2 amplitude is 7.4 cm on average, with the highest values of 14.7 ± 1.3 cm, 16.0 ± 0.7 cm, and 18.8 ± 0.7 cm found at Lusi, Haikou, and Beihai, respectively (Table 2). From Dalian to Zhapo except at Kaohsiung, the ratio of the radiational amplitude over the gravitational amplitude ranges 0.12–0.30 with an average of 0.16, and the phase differences between the two components are between 115° and 165° with an average of 134°. These results for amplitude and phase are consistent with estimates for the UK and US coasts [*Zetler*, 1971; *Amin*, 1982]. However, in the Gulf of Tonkin (at Haikou, Dongfang, and Beihai) and at Kaohsiung, the amplitude ratio goes up to 0.57–0.78, and the phase difference is nearly 180°.

In Zetler's method, the accuracy of the estimated values of the S_2 radiational component depends highly on the uncertainties in the measured values of K_2, M_2, S_2, and N_2. When the tidal estimation errors of these constituents are taken into account, however, the ratios of the radiational amplitude over the gravitational amplitude of S_2 in the Gulf of Tonkin (at Haikou, Dongfang, and Beihai) still remain much larger than the values in other regions (Table 2). Thus, we conclude that the radiational forcing is strong in this area of small semidiurnal tides.

Interannual changes in the S_2 amplitude are significantly correlated with the 18.61 year nodal cycle at 12 stations, except at Nakano, Naha, Kaohsiung, Zhapo, and Dongfang (Figure 7a). The nodal amplitude ($\alpha_{N'}$) is about 0.5 cm on average, with values higher than 0.5 cm on the northern mainland coast from Dalian to

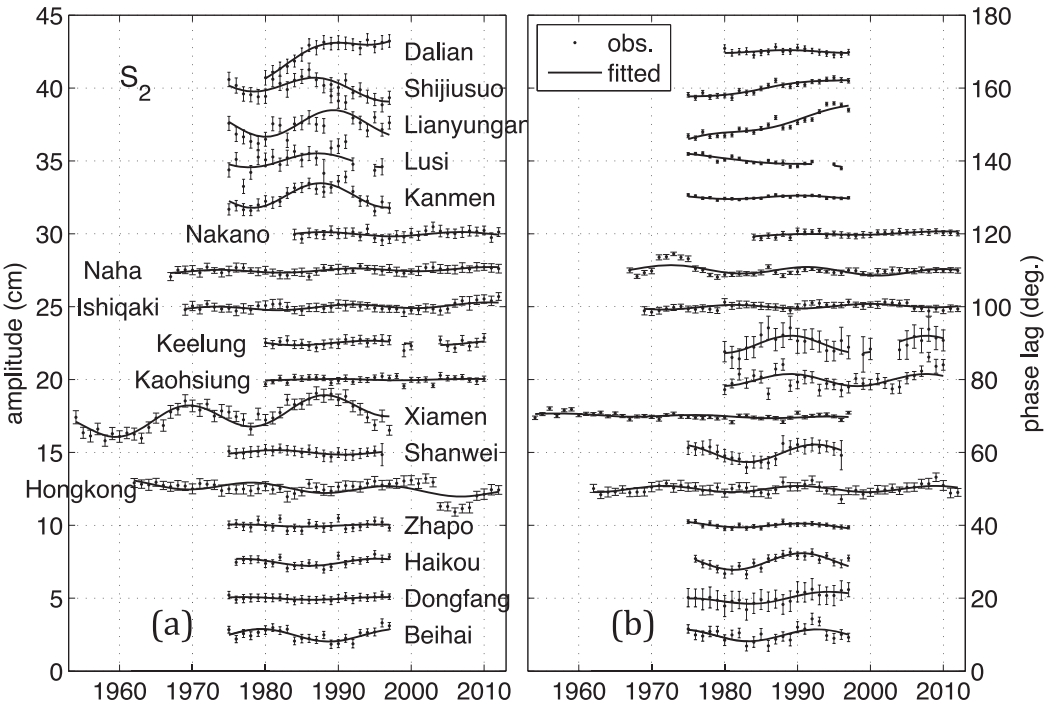

Figure 7. Same as Figure 5, but for S_2. Parameters of the best estimations (black solid lines) are presented in the supporting information Table S5.

Xiamen. The largest changes occur at Xiamen and Lianyungang with values of 0.9 ± 0.2 cm and 0.9 ± 0.4 cm, respectively. The ratios of the nodal amplitude over the S_2 amplitude ($\alpha_N'/\bar{B}$) are 1.8% on average. The changes in the S_2 phase lag also show variation with the 18.61 year cycle at 13 stations, except at Dalian, Shijiusuo, Nakano, and Xiamen (Figure 7b). The nodal cycle of the S_2 phase lag is 1.3° on average, with a maximum value of 2.4° at Shanwei. The estimation model can overall account for 57% of the variance both in the S_2 amplitude and phase lag.

Nodal modulation of the S_2 constituent has also been found at the UK coasts [*Amin*, 1983], the Gulf of Maine [*Müller*, 2011], and other coastlines with primarily semidiurnal tides [*Woodworth*, 2010], and has been attributed to shallow-water nonlinear interactions between S_2 and M_2. The nonlinear interactions between the two tidal constituents take place via their currents and the effect will also be larger when the elevations are larger in their nodal cycle. The currents will dissipate most when S_2 and M_2 are in phase [*Parker*, 2007] due to bottom friction that is approximately proportional to the square of the combined current speed [see *Pugh and Woodworth*, 2014, section 6.2.1]. The interactions result in a shallow-water tidal constituent MS_4 [*Pugh and Woodworth*, 2014, Table 4.4] that will remove energy from both M_2 and S_2. Consequently, at nodal maximum the M_2 amplitude will tend to be slightly reduced compared to equilibrium expectations, while the S_2 amplitude will also be reduced compared to its average. S_2 amplitude will, therefore, appear in 1 year analyses such as those performed here to have a nodal variation out-of-phase with M_2, as demonstrated by observations at Xiamen (Figure 8). In addition, at M_2 nodal maximum we expect the MS_4 term to also be largest.

In our data set, we find that MS_4 has an amplitude of 2.3 cm on average along the coast, with higher values in the north where the nodal changes of the S_2 amplitude are larger. At Xiamen and Lianyungang, where the average MS_4 amplitude is 5.6 cm (Figure 8) and 7.9 cm, respectively, this constituent is seen to have a nodal cycle that is in phase with that of M_2, consistent with equilibrium expectations [*Pugh and Woodworth*, 2014, Table 4.4].

Where the nodal cycle in S_2 is statistically significant, this signal is removed from the linear trend assessment. The S_2 trends are significant at Dalian and Xiamen with 1.6 ± 0.3 mm/yr and 0.4 ± 0.1 mm/yr, respectively (Figure 4a). At these two stations, when the gravitational and radiational components of S_2 are separated for every year of the observed S_2 values, the gravitational component of S_2 has significant trends

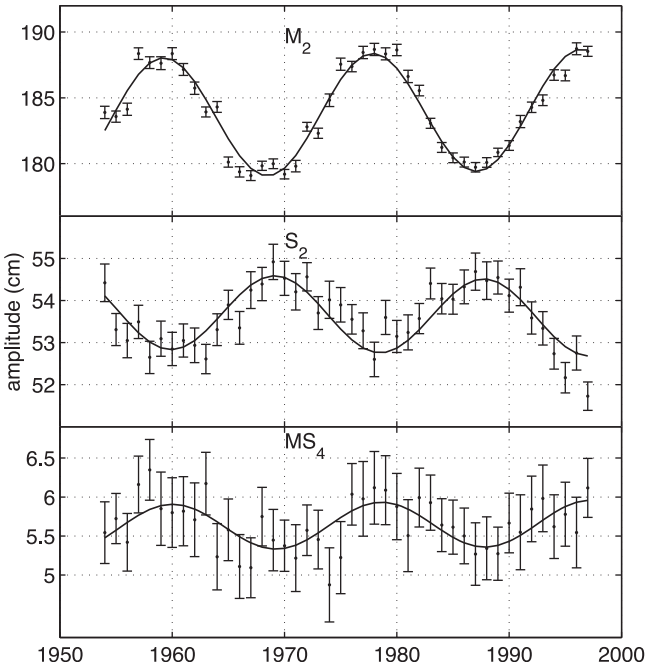

Figure 8. Amplitudes for M_2 and S_2 constituents along with the shallow-water constituent MS_4 at Xiamen. Note that the tidal amplitudes are the values after the linear trend has been removed.

of 2.1 ± 0.6 mm/yr and 0.6 ± 0.3 mm/yr, respectively, whilst no significant trend was found for the radiational component at 95% confidence level (Figure 9). Significant trends in the S_2 phase lag are found at Shijiusuo, Lianyungang, and Lusi, with values of 0.23 ± 0.05°/yr, 0.42 ± 0.08°/yr, and −0.15 ± 0.05°/yr, respectively (Figure 4b). The trends in the S_2 phase lag are found to be consistent with trends in the gravitational component as well. Therefore, we conclude that the observed linear trends in the S_2 parameters are due to the changes in the gravitational component.

4. Discussion

4.1. Possible Causes of Discrepancies in the Nodal Modulations

We found that the equilibrium theory tends to over-predict the nodal modulations of the semidiurnal tidal amplitudes of M_2 and N_2 in the Bohai, Yellow, and East China Seas. Over-prediction of the nodal modulations of M_2 by the equilibrium theory has been observed in the British Isles [*Amin*, 1983, 1985; *Woodworth et al*., 1991], the Bay of Fundy and Gulf of Maine [*Ku et al*., 1985; *Ray*, 2006; *Müller*, 2011] and western Australian coasts [*Amin*, 1993; *Woodworth*, 2010]. As mentioned above, modeling studies suggest that tidal friction with the seabed is the main cause of the reduction of the nodal modulation at semidiurnal frequencies across the North-West European Continental Shelf including the

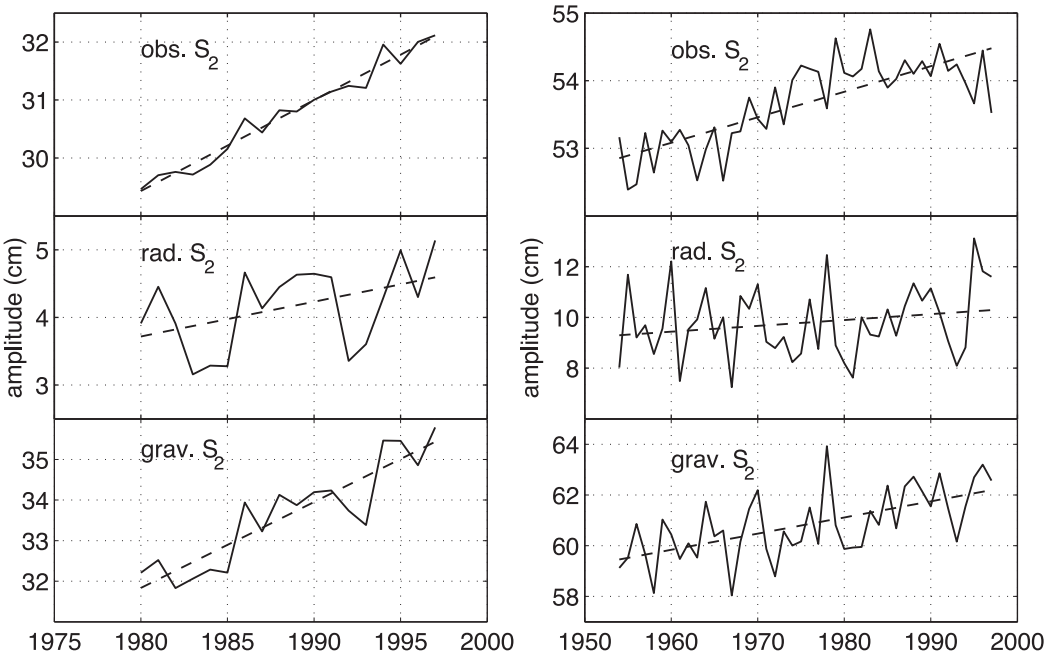

Figure 9. Amplitudes of the total (observed), radiational and gravitational S_2 at (left) Dalian and (right) Xiamen, along with their linear trends (dashed line). Note that the observed S_2 values are the values after the estimated nodal cycle has been subtracted.

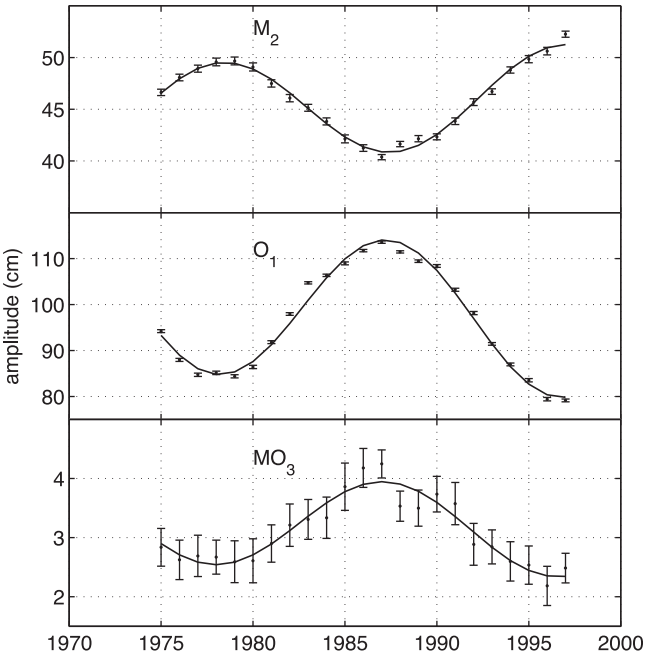

Figure 10. Amplitudes for M_2 and O_1 constituents along with the shallow-water constituent MO_3 at Beihai. Note that the tidal amplitudes are the values after the linear trend has been removed.

North Sea [*Pingree and Griffiths*, 1987], and in the Bay of Fundy and Gulf of Maine particularly under tidal resonance [*Ku et al*., 1985]. The Bohai, Yellow, and East China Seas have water depths less than 100 m and a continental shelf with widths of several hundred kilometers (Figure 1a). Thus, bottom friction effects may also be responsible for the mismatch between observed and theoretically predicted nodal variations in this area too.

The nodal modulation of M_2 and N_2 amplitudes is underestimated by the equilibrium theory in the South China Sea. *Pingree and Griffiths* [1987] suggested that the difference in the location of the tidal amphidromes of the nodal and the main M_2 components and the associated differences in the bottom friction may be the reason for the amplified nodal modulations observed in the western Irish Sea. However, because there is no amphidrome for the semidiurnal constituents in the region of the South China Sea under study here [*Fang et al*., 1999; *Hu et al*., 2001], similar mechanisms are not likely to be relevant in the present case.

We suggest that shallow-water interactions between the semidiurnal and diurnal constituents can be responsible for the observed discrepancies between the predicted and observed nodal modulations of the semidiurnal tides in the south. In the South China Sea, especially in the Gulf of Tonkin, the diurnal constituents of O_1 and K_1 are the dominating tidal signals, and the amplitudes of both constituents in the equilibrium tide have nodal variations that are out-of-phase with those in M_2. This can be seen clearly in the data from Beihai, for example (Figure 10). If we invoke a similar interaction mechanism as above for M_2 and S_2 in a semidiurnal area, the interactions in this diurnal area will result in shallow-water constituents MO_3 and MK_3. In the case of O_1 interacting with M_2, at O_1 nodal maximum, in addition to an increased MO_3 amplitude (Figure 10, bottom), there will be a slightly reduced O_1 amplitude compared to equilibrium expectations and also reduced M_2 amplitude. Similarly, at O_1 nodal minimum there will be a slightly larger M_2 amplitude. Because the nodal variations of O_1 and M_2 are out-of-phase, the interactions serve to amplify M_2's own nodal variation.

The shallow-water constituents MO_3 and MK_3 are significant throughout the South China Sea, with average values of 1.6 cm and 1.8 cm, respectively, supporting our suggestion of the importance of shallow-water interactions in modifying the nodal behavior of M_2 amplitude in this area dominated by diurnal tides.

The equilibrium nodal theory works well for O_1 and K_1 at most stations on the Chinese coast. This is consistent with what has been found in other regions [*Jay*, 2009; *Shaw and Tsimplis*, 2010; *Woodworth*, 2010; *Torres and Tsimplis*, 2011]. However, at some stations in the South China Sea, the nodal modulations are significantly overestimated by the theory. By contrast, altimetry data indicate that the observed nodal cycles in the open areas of the South China Sea are consistent with the equilibrium predictions [*Cherniawsky et al*., 2010, see their Table 2]. The agreement between the theoretical estimates and the altimetry analysis at the open sea [*Cherniawsky et al*., 2010] is consistent with the view that the deviation of the equilibrium theory from tide-gauge observations occurs primarily near the coasts, and is mainly due to interactions between the various tidal constituents.

The nodal amplitudes of the shallow-water constituents M_4, MS_4, MK_3, and MO_3 are less than 1 cm for all stations, except for M_4 at Lianyungang (1.5 ± 0.1 cm) and for MK_3 and MO_3 at Haikou (1.2 ± 0.1 cm and

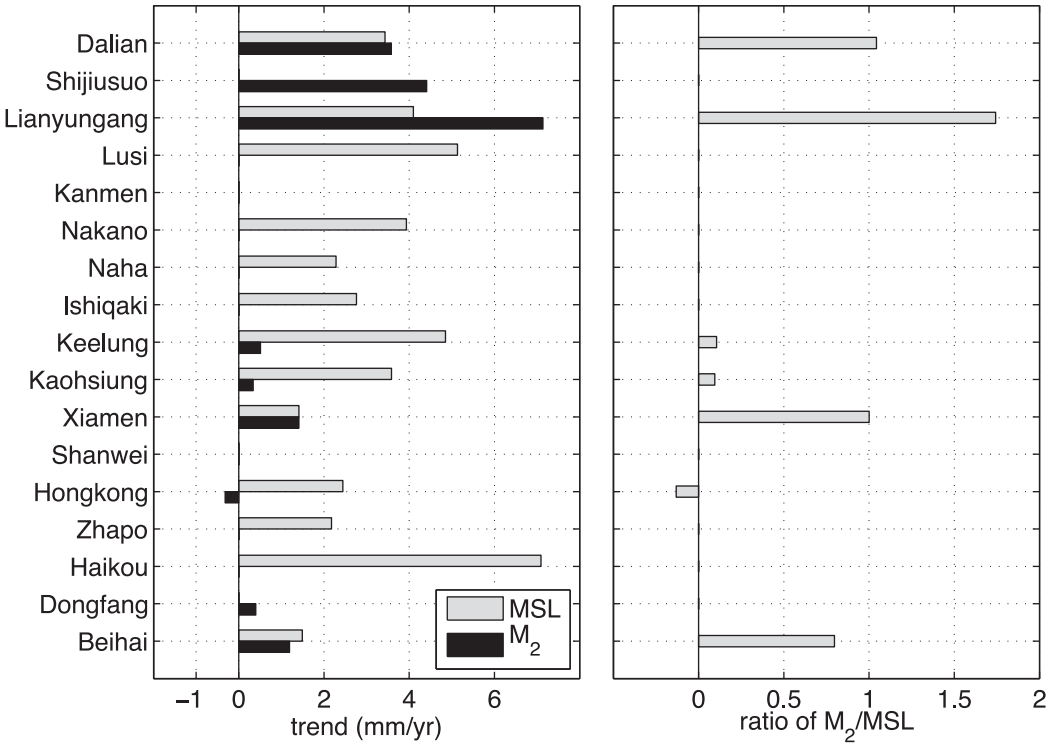

Figure 11. (left) Comparisons of significant linear trends in mean sea level (MSL) with those in the M_2 amplitude, (right) and the ratio between the two trends. Nonexistence of values at some stations indicates that the linear trends in either MSL or M_2 amplitude do not pass the significance test with 95% confidence level.

1.0 $\pm$ 0.2 cm, respectively). For these three exceptions, the ratio of nodal modulation to the mean value is 12.7 $\pm$ 1.5%, 53.7 $\pm$ 14.8%, and 56.6 $\pm$ 22.0%, respectively, which exceeds what is expected from the equilibrium theory [*Pugh and Woodworth*, 2014, see their Table 4.4].

4.2. Possible Causes of the Linear Trends

The observed trends in the M_2 constituent are problematic. Trends in tidal constituents have been identified in modeling studies under the assumption of large mean sea level (MSL) rise of the order of meters [*Amin*, 1983; *Green*, 2010; *Pickering et al*., 2012]. For the Asian coasts, the tidal changes due to MSL rise have been estimated by a numerical model in which the maximum increase of M_2 amplitude was found to be ~30 cm on the coasts of China when MSL is raised by 2 m, i.e., 15% of the MSL increase [*Pickering*, 2014, see his Figures 3.9, 3.10 and Table 3.5]. However, in observations, we find that the changes in the M_2 amplitude do not always correspond to the MSL rise (Figure 11), and the observed trends at some stations are much larger than 15% of those in MSL. In addition, the interannual variability of the M_2 amplitude was found to be uncorrelated with the interannual variability of MSL, both sets detrended (not shown here). Thus, the rates of tidal change due to the MSL rise suggested by numerical models are too small to explain the observed changes.

The rapid evolution of bathymetry in the area of study may provide another explanation for the linear trends in the tidal signal. Numerical experiments indicate that changes in coastline and bathymetry in the Bohai and Yellow Seas can significantly alter the M_2 amplitude [*Pelling et al*., 2013; *Song et al*., 2013]. Since the 1950s, significant reclamation of tidal flats has created new land areas of thousands of square km, which have changed the coastline significantly [*Li et al*., 2004; *Wang et al*., 2011; *Li et al*., 2013; *Wang et al*., 2014]. Three large river estuaries, i.e., the Yellow River, Yangtze River, and Pearl River, bring to the Bohai, East China, and South China Seas, respectively, very large amounts of sediment, which also cause significant changes in the bathymetry [*Zhang et al*., 2008; *Yang et al*., 2011; *Yu et al*., 2011]. In addition, the coastline is exposed to typhoons [*Feng et al*., 2012; *Feng and Tsimplis*, 2014] that are able to erode the shoreline and change the bathymetry [*Qi et al*., 2010; *Milliman et al*., 2007]. These changes could alter the propagation of

the tidal signal, and thus cause changes in the observed tides, including displacement of the amphidromes. However, the resolution of this issue requires numerical studies that are beyond the scope of this paper.

Finally, as suggested by one reviewer, changes in stratification could present another mechanism. In this region, a strong seasonal cycle of the tides is apparent [*Kang et al*., 2002; *Müller et al*., 2014], and could possibly be explained by the changes in stratification and thereby tidal transports. The same effect can also cause long-term changes in the tides if the stratification changes over long timescales due to climate change.

5. Conclusions

The spatiotemporal changes of the five main tidal constituents (O_1, K_1, M_2, N_2, and S_2) along the coasts of the China seas and in adjacent seas have been investigated using 17 tide-gauge records spanning the period 1954–2012. The semidiurnal tide M_2 dominates the north coast, whilst the coastline of the South China Sea is dominated by the diurnal tides. The mainland coast has higher tides than the offshore islands.

The 18.61 year nodal modulations of the main lunar constituents were identified in observations and compared with the theoretical predictions based on the tidal potential. The equilibrium theory estimates compare well with the observed nodal changes in the O_1 and K_1 parameters at most stations. However, the equilibrium theory overestimates the nodal modulations of the diurnal tidal amplitudes for the South China Sea. The discrepancy amounts up to 1–3 cm in amplitude.

The equilibrium tidal theory over-predicts the nodal modulations of the M_2 and N_2 amplitudes in the north and under-predicts them in the south. The maximum discrepancy of 3 cm was found in the Gulf of Tonkin. It has been suggested that shallow-water interactions between tidal constituents may be the cause of the discrepancies in the south. We believe this to be a plausible explanation, although it is not a proof and only more extensive measurements and modeling can provide more insight.

The nodal cycle in the N_2 amplitude and phase lag in general accounts for 17% and 15% more variance, respectively, than the perigean cycle does. The impact of perigean cycle is small in the South China Sea.

The interannual changes in the S_2 constituent are correlated significantly with the 18.61 year nodal cycle at most places. Shallow-water nonlinear interactions with M_2 are the suggested explanation.

For S_2, the contribution from radiational forcing has been separated from that of the gravitational forcing. The ratio of the radiational over the gravitational component is about 0.16 and the phase difference is 134°. These results are in agreement with results in other regions. In areas like the Gulf of Tonkin, where the semidiurnal constituents are small, the ratios obtained reach up to 0.57–0.65.

Linear changes in the amplitude and phase of the various tidal components were also examined. The records at several stations are not very long and, therefore, the linear changes found may not reflect the real long-term trends. O_1 and K_1 were found to be generally stable over the observed period, except at two stations in the South China Sea where small but significant trends were obtained. The main semidiurnal constituents show significant changes. The M_2 amplitude, in particular, increases at 9 of the 17 stations, and the N_2 and S_2 amplitudes increase also at a few stations. The highest changes for M_2, with rates between 3 and 7 mm/yr, were found in the Bohai and Yellow Seas. Rates of 0.3–1.4 mm/yr were found in the Taiwan Strait. The phase lags of the semidiurnal constituents were found to be changing in time as well, getting smaller at Bohai and East China Seas, but progressively larger in the Yellow Sea.

We found no convincing evidence supporting a link between the linear tidal changes and MSL rise. We suspect changes in tidal wave propagation, due to the rapid evolution of the coastal bathymetry caused by natural and anthropogenic processes, as the main cause for these changes.

Land reclamation along the Chinese coasts has been intensive for the last few decades, and is expected to continue in the future, with even higher intensity. Around 6000 km^2 of land, in terms of coastal reclamations and artificial offshore islands, is planned to be built in the next 10 years [*Joss and Molella*, 2013; *Wang et al*., 2014, and references therein]. The significant expansion of land raises serious concerns for potential changes in the tidal environment. Flood risks, which depend on MSL rise and the combination of typhoons and tides [*Feng and Tsimplis*, 2014], are likely to become more uncertain.

Acknowledgments
This research is funded by Lloyd's Register Foundation, which supports the advancement of engineering-related education, and funds research and development that enhances safety of life at sea, on land and in the air. Data used in the paper were obtained from the University of Hawaii Sea Level Center (UHSLC) (http://ilikai.soest.hawaii.edu/uhslc). We thank M. G. G. Foreman for making his tidal analysis and prediction programs publicly available, and thank three reviewers and A. P. G. Shaw as well for their constructive comments and suggestions.

References

Amin, M. (1982), On analysis and prediction of tides on the west coast of Great Britain, *Geophys. J. Int.*, *68*(1), 57–78, doi:10.1111/j.1365-246X.1982.tb06962.

Amin, M. (1983), On perturbations of harmonic constants in the Thames Estuary, *Geophys. J. Int.*, *73*(3), 587–603, doi:10.1111/j.1365-246X.1983.tb03334.

Amin, M. (1985), Temporal variations of tides on the west coast of Great Britain, *Geophys. J. R. Astron. Soc.*, *82*, 279–299, doi:10.1111/j.1365-246X.1985.tb05138.x.

Amin, M. (1993), Changing mean sea level and tidal constants on the west coast of Australia, *Mar. Freshwater Res.*, *44*(6), 911–925, doi:10.1071/MF9930911.

Arbic, B. K. (2005), Atmospheric forcing of the oceanic semidiurnal tide, *Geophys. Res. Lett.*, *32*, L02610, doi:10.1029/2004GL021668.

Cartwright, D. E. (1968), A unified analysis of tides and surges round north and east Britain, *Philos. Trans. R. Soc. London A*, *263*, 1–55, doi:10.1098/rsta.1968.0005.

Cartwright, D. E., and A. C. Edden (1973), Corrected tables of tidal harmonics, *Geophys. J. R. Astron. Soc.*, *33*(3), 253–264, doi:10.1111/j.1365-246X.1973.tb03420.x.

Cartwright, D. E., and R. J. Tayler (1971), New computations of the tide-generating potential, *Geophys. J. Int.*, *23*(1), 45–73, doi:10.1111/j.1365-246X.1971.tb01803.

Chapman, S., and R. S. Lindzen (1970), *Atmospheric Tides: Thermal and Gravitational*, vol. 15, Springer, Dordrecht, Holland.

Cherniawsky, J. Y., M. G. Foreman, S. K. Kang, R. Scharroo, and A. J. Eert (2010), 18.6-year lunar nodal tides from altimeter data, *Cont. Shelf Res.*, *30*(6), 575–587, doi:10.1016/j.csr.2009.10.002.

Chu, Z. X., X. G. Sun, S. K. Zhai, and K. H. Xu (2006), Changing pattern of accretion/erosion of the modern Yellow River (Huanghe) subaerial delta, China: Based on remote sensing images, *Mar. Geol.*, *227*(1), 13–30, doi:10.1016/j.margeo.2005.11.013.

Darwin, G. H., and J. C. Adams (1883), Report of a Committee, consisting of Professors G. H. Darwin and J. C. Adams, for the harmonic analysis of tidal observations, *Br. Assoc. for the Adv. of Sci. Rep. for 1883*, pp. 49–117.

Ding, X., D. Zheng, Y. Chen, J. Chao, and Z. Li (2001), Sea level change in Hong Kong from tide gauge measurements of 1954–1999, *J. Geod.*, *74*(10), 683–689, doi:10.1007/s001900000128.

Doodson, A. T. (1928), The analysis of tidal observations, *Philos. Trans. R. Soc. London A*, *227*, 223–279.

Doodson, A. T., and H. D. Warburg (1941), *Admiralty Manual of Tides*, Her Majesty's Stn. Off., London, U. K.

Fang, G. (1986), Tide and tidal current charts for the marginal seas adjacent to China, *Chin. J. Oceanol. Limnol.*, *4*(1), 1–16, doi:10.1007/BF02850393.

Fang, G. (1994), *Tides and Tidal Currents in East China Sea, Huanghai Sea and Bohai Sea, Oceanology of China Seas*, pp. 101–112, Springer, Netherlands, doi:10.1007/978-94-011–0862-1_11.

Fang, G., Y. K. Kwok, K. Yu, and Y. Zhu (1999), Numerical simulation of principal tidal constituents in the South China Sea, Gulf of Tonkin and Gulf of Thailand, *Cont. Shelf Res.*, *19*(7), 845–869, doi:10.1016/S0278–4343(99)00002–3.

Fang, G., Y. Wang, Z. Wei, B. H. Choi, X. Wang, and J. Wang (2004), Empirical cotidal charts of the Bohai, Yellow, and East China Seas from 10 years of TOPEX/Poseidon altimetry, *J. Geophys. Res.*, *109*, C11006, doi:10.1029/2004JC002484.

Feng, X., and M. N. Tsimplis (2014), Sea level extremes at the coasts of China, *J. Geophys. Res. Oceans*, *119*, 1593–1608, doi:10.1002/2013JC009607.

Feng, X., J. Zheng, and Y. Yan (2012), Wave spectra assimilation in typhoon wave modeling for the East China Sea, *Coastal Eng.*, *69*, 29–41, doi:10.1016/j.coastaleng.2012.05.007.

Foreman, M. G. G. (1977), Manual for tidal heights analysis and prediction, *Pac. Mar. Sci. Rep. 77-10*, 97 pp., Inst. of Ocean Sci., Patricia Bay, Sidney, B. C.

Godin, G. (1972), *The Analysis of Tides*, 264 pp., Univ. of Toronto Press, Toronto, Canada.

Green, J. A. M. (2010), Ocean tides and resonance, *Ocean Dyn.*, *60*(5), 1243–1253, doi:10.1007/s10236-010-0331-1.

Haigh, I. D., M. Eliot, and C. Pattiaratchi (2011), Global influences of the 18.61 year nodal cycle and 8.85 year cycle of lunar perigee on high tidal levels, *J. Geophys. Res. Oceans*, *116*, C06025, doi:10.1029/2010JC006645.

He, Y., X. Lu, Z. Qiu, and J. Zhao (2004), Shallow water tidal constituents in the Bohai Sea and the Yellow Sea from a numerical adjoint model with TOPEX/POSEIDON altimeter data, *Cont. Shelf Res.*, *24*(13), 1521–1529, doi:10.1016/j.csr.2004.05.008.

Hollebrandse, F. A. (2005), Temporal development of the tidal range in the southern North Sea, MSc thesis, Delft Univ. of Technol., Delft, Netherlands.

Hu, J. Y., H. Kawamura, H. S. Hong, F. Kobashi, and Q. Xie (2001), Tidal features in the China Seas and their adjacent sea areas as derived from TOPEX/POSEIDON altimeter data, *Chin. J. Oceanol. Limnol.*, *19*, 293–305, doi:10.1007/BF02850732.

Jan, S., C. S. Chern, J. Wang, and S. Y. Chao (2004), The anomalous amplification of M2 tide in the Taiwan Strait, *Geophys. Res. Lett.*, *31*, L07308, doi:10.1029/2003GL019373.

Jay, D. A. (2009), Evolution of tidal amplitudes in the eastern Pacific Ocean, *Geophys. Res. Lett.*, *36*, L04603, doi:10.1029/2008GL036185.

Joss, S., and A. P. Molella (2013), The eco-city as urban technology: Perspectives on Caofeidian international eco-city (China), *J. Urban Technol.*, *20*(1), 115–137, doi:10.1080/10630732.2012.735411.

Kang, S. K., S. R. Lee, and H. J. Lie (1998), Fine grid tidal modeling of the Yellow and East China Seas, *Cont. Shelf Res.*, *18*(7), 739–772, doi:10.1016/S0278–4343(98)00014-4.

Kang, S. K., M. G. G. Foreman, H.-J. Lie, J.-H. Lee, J. Cherniawsky, and K.-D. Yum (2002), Two-layer tidal modeling of the Yellow and East China Seas with application to seasonal variability of the M_2 tide, *J. Geophys. Res.*, *107*(C3), 3020, doi:10.1029/2001JC000838.

Ku, L. F., D. A. Greenberg, C. J. R. Garrett, and F. W. Dobson (1985), Nodal modulation of the lunar semidiurnal tide in the Bay of Fundy and Gulf of Maine, *Science*, *230*(4721), 69–71, doi:10.1126/science.230.4721.69.

Lefèvre, F., C. Le Provost, and F. H. Lyard (2000), How can we improve a global ocean tide model at a regional scale? A test on the Yellow Sea and the East China Sea, *J. Geophys. Res.*, *105*(C4), 8707–8725, doi:10.1029/1999JC900281.

Li, C., D. Fan, B. Deng, and V. Korotaev (2004), The coasts of China and issues of sea level rise, *J. Coastal Res.*, *43*, 36–49.

Li, Y., Y. Shi, X. Zhu, H. Cao, and T. Yu (2013), Coastal wetland loss and environmental change due to rapid urban expansion in Lianyungang, Jiangsu, China, *Reg. Environ. Change*, *14*(3), 1175–1188, doi:10.1007/s10113-013-0552-1.

Milliman, J. D., S. W. Lin, S. J. Kao, J. P. Liu, C. S. Liu, J. K. Chiu, and Y. C. Lin (2007), Short-term changes in seafloor character due to flood-derived hyperpycnal discharge: Typhoon Mindulle, Taiwan, July 2004, *Geology*, *35*(9), 779–782, doi:10.1130/G23760A.1.

Müller, M. (2011), Rapid change in semi-diurnal tides in the North Atlantic since 1980, *Geophys. Res. Lett.*, *38*, L11602, doi:10.1029/2011GL047312.

Müller, M. (2012), The influence of changing stratification conditions on barotropic tidal transport and its implications for seasonal and secular changes of tides, *Cont. Shelf Res.*, *47*, 107–118, doi:10.1016/j.csr.2012.07.003.
Müller, M., B. K. Arbic, and J. X. Mitrovica (2011), Secular trends in ocean tides: Observations and model results, *J. Geophys. Res.*, *116*, C05013, doi:10.1029/2010JC006387.
Müller, M., J. Cherniawsky, M. Foreman, and J.-S. von Storch (2014), Seasonal variation of the M2 tide, *Ocean Dyn.*, *64*(2), 159–177, doi:10.1007/s10236-013-0679-0.
Munk, W. H., and D. E. Cartwright (1966), Tidal spectroscopy and prediction, *Philos. Trans. R. Soc. London A*, *259*, 533–581, doi:10.1098/rsta.1966.0024.
Parker, B. B. (2007), *Tidal Analysis and Prediction*, NOAA Special Publication NOS CO-OPS 3, US Department of Commerce, 378 pp., Silver Spring, Md.
Pelling, H. E., K. Uehara, and J. A. M. Green (2013), The impact of rapid coastline changes and sea level rise on the tides in the Bohai Sea, China, *J. Geophys. Res. Oceans*, *118*, 3462–3472, doi:10.1002/jgrc.20258.
Pickering, M. D. (2014), The impact of future sea-level rise on the tides, Doctoral thesis, Univ. of Southampton, Southampton, U. K.
Pickering, M. D., N. C. Wells, K. J. Horsburgh, and J. A. M. Green (2012), The impact of future sea-level rise on the European Shelf tides, *Cont. Shelf Res.*, *35*, 1–15, doi:10.1016/j.csr.2011.11.011.
Pingree, R. D., and D. K. Griffiths (1987), Tidal friction for semidiurnal tides, *Cont. Shelf Res.*, *7*(10), 1181–1209, doi:10.1016/0278–4343(87)90084-7.
Pugh, D., and P. Woodworth, (2014), *Sea-Level Science: Understanding Tides, Surges, Tsunamis and Mean Sea-Level Changes*, 395 pp., Cambridge Univ. Press, Cambridge, U. K.
Qi, H., F. Cai, G. Lei, H. Cao, and F. Shi (2010), The response of three main beach types to tropical storms in South China, *Mar. Geol.*, *275*(1), 244–254, doi:10.1016/j.margeo.2010.06.005.
Ray, R. D. (2006), Secular changes of the M2 tide in the Gulf of Maine, *Cont. Shelf Res.*, *26*(3), 422–427, doi:10.1016/j.csr.2005.12.005.
Ray, R. D. (2009), Secular changes in the solar semidiurnal tide of the western North Atlantic Ocean, *Geophys. Res. Lett.*, *36*, L19601, doi:10.1029/2009GL040217.
Shaw, A. G. P., and M. N. Tsimplis (2010), The 18.6 yr nodal modulation in the tides of southern European coasts, *Cont. Shelf Res.*, *30*(2), 138–151, doi:10.1016/j.csr.2009.10.006.
Song, D., X. Wang, X. Zhu, and X. Bao (2013), Modeling studies of the far-field effects of tidal flat reclamation on tidal dynamics in the East China Seas, *Estuarine Coastal Shelf Sci.*, *133*, 147–160, doi:10.1016/j.ecss.2013.08.023.
Torres, R. R., and M. N. Tsimplis (2011), Tides and long-term modulations in the Caribbean Sea, *J. Geophys. Res.*, *116*, C10022, doi:10.1029/2011JC006973.
Wang, W., H. Liu, Y. Li, and J. Su (2014), Development and management of land reclamation in China, *Ocean Coastal Manage.*, *102*, 415–425, doi:10.1016/j.ocecoaman.2014.03.009.
Wang, Y. P., S. Gao, J. Jia, C. E. Thompson, J. Gao, and Y. Yang (2011), Sediment transport over an accretional intertidal flat with influences of reclamation, Jiangsu coast, China, *Mar. Geol.*, *291*, 147–161, doi:10.1016/j.margeo.2011.01.004.
Woodworth, P. L. (2010), A survey of recent changes in the main components of the ocean tide, *Cont. Shelf Res.*, *30*(15), 1680–1691, doi:10.1016/j.csr.2010.07.002.
Woodworth, P. L., S. M. Shaw, and D. L. Blackman (1991), Secular trends in mean tidal range around the British Isles and along the adjacent European coastline, *Geophys. J. Int.*, *104*(3), 593–609, doi:10.1111/j.1365-246X.1991.tb05704.x.
Yang, S. L., J. D. Milliman, P. Li, and K. Xu (2011), 50,000 dams later: Erosion of the Yangtze River and its delta, *Global Planet. Change*, *75*(1), 14–20, doi:10.1016/j.gloplacha.2010.09.006.
Yu, J., Y. Fu, Y. Li, G. Han, Y. Wang, D. Zhou, and F. X. Meixner (2011), Effects of water discharge and sediment load on evolution of modern Yellow River Delta, China, over the period from 1976 to 2009, *Biogeosci. Discuss.*, *8*, 4107–4130, doi:10.5194/bg-8–2427-2011.
Zetler, B. D. (1971), Radiational ocean tides along the coasts of the United States, *J. Phys. Oceanogr.*, *1*(1), 34–38, doi:10.1175/1520-0485(1971)001<0032:ROTATC>2.0.CO;2.
Zhang, S., X. X. Lu, D. L. Higgitt, C. T. A. Chen, J. Han, and H. Sun (2008), Recent changes of water discharge and sediment load in the Zhujiang (Pearl River) Basin, China, *Global Planet. Change*, *60*(3), 365–380, doi:10.1016/j.gloplacha.2007.04.003.
Zu, T., J. Gan, and S. Y. Erofeeva (2008), Numerical study of the tide and tidal dynamics in the South China Sea, *Deep Sea Res., Part I*, *55*(2), 137–154, doi:10.1016/j.dsr.2007.10.007.

Erratum

In the originally published version of this article, there were minor typos in the headings of Table 2 and on top of Figure 10. The figure and the table have since been corrected, and this version may be considered the authoritative version of record.